In situ measurements of snow surface roughness using a laser profiler

Pascal Lacroix, Benoit Legrésy, K. Langley, S.E. Hamran, J. Kohler, S. Roques, Frédérique Rémy, Monique Dechambre

Instruments and Methods

In situ measurements of snow surface roughness using a laser profiler

P. LACROIX,[1] B. LEGRÉSY,[1] K. LANGLEY,[2] S.E. HAMRAN,[2] J. KOHLER,[3] S. ROQUES,[4] F. RÉMY,[1] M. DECHAMBRE[5]

[1]*Legos, 18 av. Edouard Belin, 31401 Toulouse Cedex, France*
E-mail: Pascal.Lacroix@legos.obs-mip.fr
[2]*University of Oslo, PO Box 1042, Blindern, NO-0316 Oslo, Norway*
[3]*Norwegian Polar Institute, Polarmiljøsenteret, NO-9296 Tromsø, Norway*
[4]*Laboratoire d'Astrophysique de Toulouse-Tarbes, 18 av. Edouard Belin, 31401 Toulouse Cedex, France*
[5]*Centre d'Etude des Environnements Terrestres et Planétaires, 10–12 av. de l'Europe, 78140 Vélizy-Villacoublay Cedex, France*

ABSTRACT. The snow surface roughness at centimetre and millimetre scales is an important parameter related to wind transport, snowdrifts, snowfall, snowmelt and snow grain size. Knowledge of the snow surface roughness is also of high interest for analyzing the signal from radar sensors such as SAR, altimeters and scatterometers. Unfortunately, this parameter has seldom been measured over snow surfaces. The techniques used to measure the roughness of other surfaces, such as agricultural or sand soils, are difficult to implement in polar regions because of the harsh climatic conditions. In this paper we develop a device based on a laser profiler coupled with a GPS receiver on board a snowmobile. This instrumentation was tested successfully in midre Lovénbreen, Svalbard, in April 2006. It allowed us to generate profiles of 3 km sections of the snow-covered glacier surface. Because of the motion of the snowmobile, the roughness signal is mixed with the snowmobile signal. We use a distance/frequency analysis (the empirical mode decomposition) to filter the signal. This method allows us to recover the snow surface structures of wavelengths between 4 and 50 cm with amplitudes of >1 mm. Finally, the roughness parameters of snow surfaces are retrieved. The snow surface roughness is found to be dependent on the scales of the observations. The retrieved RMS of the height distribution is found to vary between 0.5 and 9.2 mm, and the correlation length is found to be between 0.6 and 46 cm. This range of measurements is particularly well adapted to the analysis of GHz radar response on snow surfaces.

INTRODUCTION

Microreliefs on the snow surface are formed by a process of erosion and redeposition of the snow by the wind. Roughness is thus an important indicator related to wind transport (strong winds form sastrugi), temperature and snowfall. The roughness of snow surfaces is an important control on air–snow heat transfer (Munro, 1989), on the snow surface albedo and thus on the surface energy balance. The aerodynamic roughness length that accounts for energy balance is defined in terms of the air velocity profile near the surface. This is related to the mathematical definition of the surface roughness (Bagnold, 1941), which is measured directly from the topography of the surface. Knowledge of the surface roughness is therefore of great interest for energy-balance studies. In the following, the term 'roughness' refers exclusively to the mathematical definition of the roughness.

The radar return on ice sheets and glaciers is also highly dependent on the snow surface roughness. The backscattering coefficient decreases with increasing radar look angle. The surface radiation pattern (the diagram of scattered radiation versus incidence angle) is governed by the surface roughness at scales of fractions of the radar wavelength (Ulaby and others, 1982). This parameter is a major contribution to the synthetic aperture radar (SAR) signal (Oveisgharan and Zebker, 2007). Rees and Arnold (2006) show that the SAR backscattering coefficient at C band from a glacier surface is consistent with snow roughness at the millimetre scale. Radar altimeter signals are also very sensitive to the snow surface roughness, affecting both the backscattering coefficient and the shape of the received echo (Ridley and Partington, 1988; Legrésy and Remy, 1997; Lacroix and others, 2008). The altimetric radar signal at S and Ku band is highly dependent on the surface radiation pattern (Lacroix and others, 2007), determined by the snow surface roughness at millimetre and centimetre scales. Knowledge of the snow surface roughness at these scales is therefore of high interest for analyzing radar signals at GHz frequencies over snow surfaces (Lacroix and others, 2008).

Unfortunately, the roughness of snow surfaces is a relatively unknown parameter. As yet, few measurements of snow surface roughness have been undertaken. To the best of our knowledge, measurements of snow surface roughness started with observations of millimetre-scale variations in snow surface topography, by comparing the snow surface height with an arbitrary reference level (Rott, 1984; Williams and others, 1988). The reference level is taken to be the top of a long thin black plate. The plate is inserted into the snow and the profile of the snow is sampled every 10 cm by measuring the height between the snow surface and the horizontal top of the plate. The processing of this technique was improved by Rees (1998), and later used by Albert and Hawley (2002) at Summit, Greenland and by Rees and Arnold (2006) on midre Lovénbreen, Svalbard. Other measurements of snow

surface profiles were performed with a rill meter. This instrument is a 2 m long horizontal rod supporting vertical needles every centimetre. The needles take on the snow topography. They are locked and a picture is taken that is later digitized to provide the snow profile. Use of the rill meter was pioneered by M. Fily (personal communication, 1995) at Dome C, Antarctica in 1995 and by Bingham (1998).

Other techniques include the Glacier Roughness Sensor (GRS; Herzfeld and others, 2003), and two-dimensional retrieval of surface topography using stereo photos (personal communication from C. Vincent, 1995). The GRS consists of eight mechanical arms hinged on a main crossbar that are pulled over the snow surface. Furukawa and Young (1997) obtained a qualitative measurement of the roughness along a traverse route in Dronning Maud Land, Antarctica, by counting the occurrence of large and small sastrugi every 2 km.

Small-scale roughness measurements are difficult to obtain on snow surfaces, due to the logistic difficulties of transporting bulky instrumentation in harsh climatic conditions. Moreover, the rill meter, or the metre-long black plate, only provides knowledge of roughness over short transects. Stereo-photo measurements require the use of a calibration grid, again not easy to manipulate in such areas. Furthermore, the post-processing of all these methods is time-consuming. The GRS can provide snow surface profiles over profiles of several tens of metres, but under loose snow conditions the mechanical arms sink into the snow. Moreover, the sampling rate (1 point every 10 cm) only allows for decimetre-scale roughness studies.

Aircraft-borne lidar measurements have been used over snow surfaces, and also provide decimetre roughness scale (Rees and Arnold, 2006). For smaller scales of roughness, the laser has been used on other surfaces such as sand soils (Grandjean and others, 2001) or agricultural soils (Davidson and others, 2000). The laser is fixed on a cart that moves on rails previously installed over the surface to be measured. The equipment is thus heavy and the transect length is limited to the rail length. With the hard climatic conditions of the Antarctic and Greenland ice sheets, such measurements are impossible. Moreover, the roughness varies greatly at metre or greater scales, so requires measurements to be performed over a large area.

During the spring season of 2006, we performed profiles on a snow-covered glacier in Svalbard using a laser device. We operated the laser on board a sledge pulled by a snowmobile. This allowed us to profile long transects and avoid the heavy rail support. The relative simplicity of this method makes it a viable method for measuring snow surface roughness in polar regions. In this paper, we first present the instrumentation and then show that the laser profiles contain the snow surface signal mixed with the snowmobile movement signal. We finally propose a method to decouple these two signals, allowing the small-scale snow surface roughness to be extracted from the profiles.

MEASUREMENTS

Field site

Preliminary tests of the method and protocol were made on the Amery Ice Shelf snow and on the plateau near Davis station, Antarctica, in 2005/06. During these tests, the snowmobile regularly broke through the existing wind crust and subsided into the snow. This prohibited use of the data. The data presented here were collected during the 2006 field season, on 27 April. The field site is the glacier midre Lovénbreen situated at 78° N on the northwest of the Spitsbergen archipelago. Its location, close to the scientific station of Ny-Ålesund, makes it easy to access as a field of experimentation. Midre Lovénbreen is a partly temperate glacier with an area of 6 km^2, which drains northwards from an elevation of 550 m to about 50 m a.s.l. The slope ranges from 0 to 15%. Weather for the duration of the field campaign was relatively warm (0–7°C at the Ny-Ålesund-weather station, at sea level) and dry. This warmth and lack of snow precipitation in the previous days made the snow surface relatively smooth. No sastrugi were observed. The snowpack was compacted and dry, so the snowmobile did not sink into the snow (Fig. 1). The surface of the snow was also dry and no melt ponds were observed.

Instrumentation

The laser (ACUITY AR600-32) operates at 670 nm with infrared upgrade to avoid the impact of sunlight on the laser. Due to the laser wavelength, the radiation does not penetrate into the snowpack and is sensitive only to the surface. The user's manual (available online on http://www.acuitylaser.com/pdf/ar600-users-manual.pdf) states that the instrument works for temperatures greater than –10°C. In case of lower temperatures, the instrument must be isolated from the air outside. The cost of such a device is around €6000.

The laser is attached to a sledge behind the snow scooter (Fig. 1a), to avoid direct vibrations from the scooter. It looks to the side of the sledge rather than vertically, to avoid 'seeing' the sledge tracks (Fig. 1b). The laser measurements are coupled to a global positioning system (GPS) output to provide the location of the snow scooter (Fig. 1b). The GPS was used in differential mode, with a base station located at Ny-Ålesund scientific station (baseline of <5 km).

The sampling rate of the laser was set to 120 Hz. This rate can theoretically be set up to 1250 Hz. Depending on the nature of the surface (rough, smooth, dry, wet, white, black), the minimum sampling rate will change, as a certain amount of returned energy is required to do the measurement. The snow scooter (four-stroke Arctic Cat) was driven slowly at around 1 m s^{-1}. A lower speed produced more vibration, and could not be reasonably handled. The laser was connected to a laptop computer dedicated to data storage. Synchronization between the GPS and the laser was achieved by starting the laser measurements before the snow scooter began moving. In this way, movement of the snow scooter is seen in both the laser and the GPS records. The relation between the recording time and the distance driven is easily made using the GPS measurements performed at 1 Hz. We reformatted the laser signal to sample at regular distances, one every centimetre.

The measurements were performed over two transects with a 30 min delay, the first transect over 700 m uphill, the second over 3200 m downhill. Despite the fact that the different trajectories do not allow direct comparison of the two profiles, it is possible to compare roughness statistics, since the two transects are never separated by more than 30 m.

Protocol

To validate the laser measurements on the snow:

1. We first characterize the snowmobile vibrations by looking at the measurement variability when the engine is switched on but the snowmobile is not in motion. The

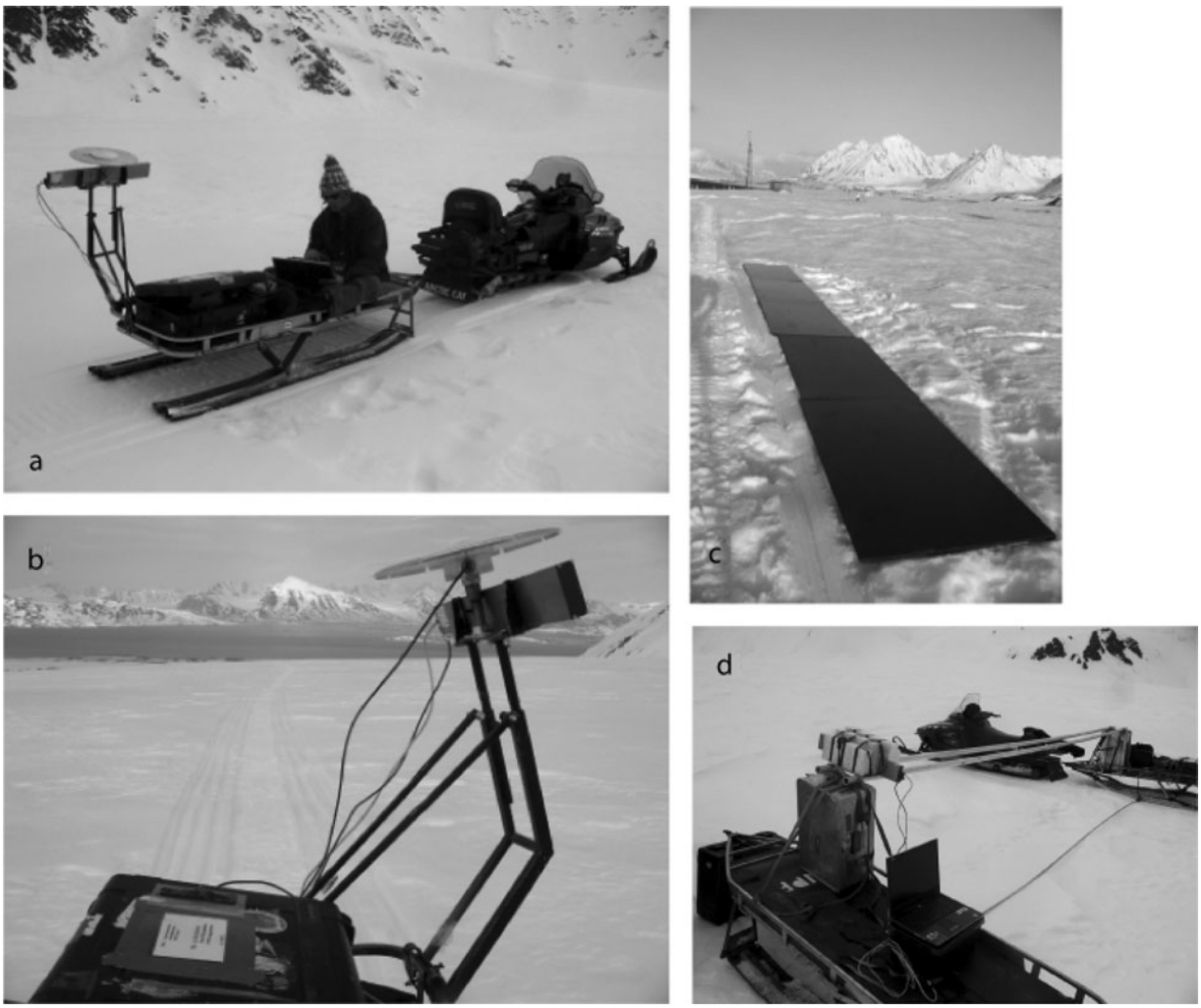

Fig. 1. Pictures of the set-up: (a) general overview of operations; (b) laser and GPS set-up; (c) wooden plate used for the calibration; and (d) laser measurements made on poles.

laser measurements vary within 1 mm, with a standard deviation of 0.2 mm. This high-frequency noise is difficult to subtract from the signal, due also to the high-frequency characteristics of the roughness signal. The effect of the engine vibrations was previously tested at different power on the Amery Ice Shelf. The results show that an engine working harder creates higher-frequency noise but no difference in signal amplitude. Therefore, the value of 1 mm provides a good estimate of the validity range for the measured signal.

2. We compare the laser signal and the GPS measurements when the snowmobile moves. For display purposes, a 10° polynomial is fitted and subtracted from the altitude GPS data every 100 m along the profile, in order to remove the large-scale topography. This comparison shows that the sledge is not stable and moves with the metre-scale topography (Fig. 2). These oscillations must be removed from the signal to provide the roughness signal.

3. The laser on board the snow scooter is then operated on a 7 m wooden plate, which provides a reference for the system, because of its very flat aspect (Fig. 1c). The signal is acquired five times on this artificial surface at different speeds (0.75–2.6 m s^{-1}). We first present a comparison of the 5 profiles on the wooden board to show how the roughness signal can be extracted. From this comparison, we propose a processing of the signal based on the empirical mode decomposition (EMD; Huang and others, 1998). The acquisition at different speeds allows us to check that the method is independent of the snow-scooter velocity (and thus the engine vibrations).

4. Then the methodology developed on the board is applied to the data on the snow. We compare the signal spectrums on the snow and on the board to evaluate the frequency validity of the processing.

5. The extracted snow surface-roughness signal is later compared to snow surface profiles realized with a laser, where the laser is not installed on the snow scooter but is translated onto two fixed parallel poles (Fig. 1d). The poles sag under their own weight, and a 2° polynomial is removed from the data to eliminate this effect. The whole measurements represent the snow surface topography, and their frequency spectrum fully characterizes the snow surface signature. Because of the fixed support, the measurements on the poles are only performed over three different transects, each 4 m long.

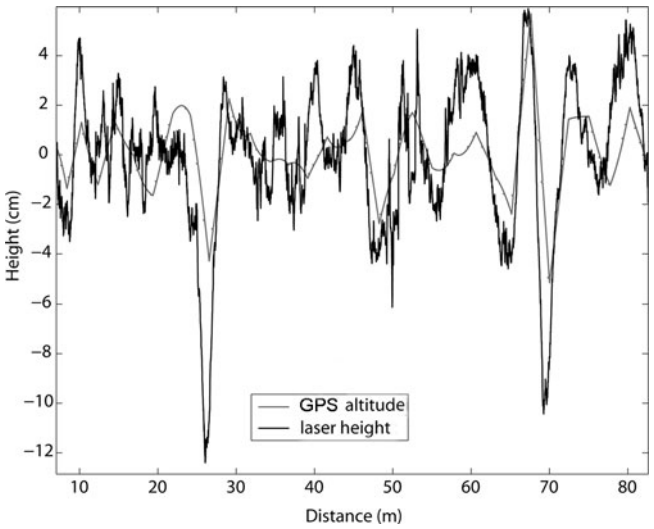

Fig. 2. Raw measurements of the laser height (black) and the GPS altitude (red), where a polynomial has been removed to mask the long-scale topography.

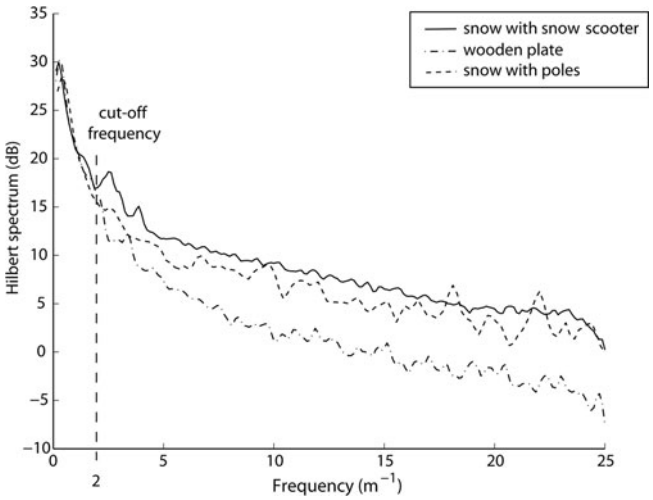

Fig. 3. Hilbert spectrum of the different profiles made with the laser on board the snowmobile (over snow (solid line), over wooden plate (dash-dotted line) and manually (dashed line)).

METHODOLOGY

First analysis

We first compare the spectral signature of the signals on the board and on the snow (Fig. 3). We clearly see that the high-frequency snow signal has much higher amplitudes than the high-frequency board signal. On the other hand, the lower frequencies have very similar signatures on the two different surfaces. This first frequency analysis proves that the laser measurement contains the high-frequency spectral signature of the snow surfaces.

We notice a difference of 3–10 dB between the high-frequency signal on the snow and the board surfaces. The frequency limit is fuzzy but is ~2–3 m^{-1}. Thus the equipment proposed here allows the retrieval of the spectral signature of snow surfaces for frequencies above 2 m^{-1} (or wavelengths below 50 cm). This wavelength limit is very well adapted to radar signal analysis.

A classical linear filter could be used to decouple the snow signature from the sledge movements for frequencies higher than 2 m^{-1}. However, the signal is not necessarily stationary, with amplitudes and frequencies depending on the small-scale surface roughness and the interaction of the sledge with the metre-scale topography. Thus, to extract the maximum roughness signal, we choose here to proceed with a scale-frequency analysis of the signal and propose to use EMD (Huang and others, 1998).

Empirical mode decomposition processing

EMD is a signal-processing method well adapted to non-linear and non-stationary data analysis. EMD has now been used for a wide variety of geophysical applications, analysis of ocean wave data (Hwang and others, 2003), of polar ice-cover data (Gloersen and Huang, 2003), of seismological data (Zhang and others, 2003), of climatic data (Molla and others, 2006) and of radiometric time series on ice sheets (Bindschadler and others, 2005).

The principle of EMD is to decompose a signal into a sum of oscillatory functions, namely intrinsic mode functions (IMF). The major advantage of this method is that the basis functions are derived directly from the signal itself. Hence, the analysis is adaptive and local, in contrast to Fourier analysis, where the basis functions are linear combinations of fixed sinusoids (approximation to a stationary signal). The IMF (1) have the same number of zero-crossings or differ at most by one; and (2) are symmetric with respect to local zero mean. These two conditions allow the calculation of a meaningful instantaneous frequency.

The IMF are calculated as follows (Huang and others, 1998):

1. Identify the extrema (both maxima and minima) of the signal $s(x)$.
2. Generate the envelope by connecting maxima points with a cubic spline (and the same for the minima points).
3. Determine the mean envelope $m(x)$ by averaging the minima and maxima envelopes.
4. Subtract out the mean envelope from the signal $g(x) = s(x) - m(x)$.
5. Iterate steps 1–4 until the mean envelope reaches the criterion of convergence.
6. The resulting IMF is the signal $g(x)$.
7. Steps 1–6 are iterated with the resulting signal $s(x) = s(x) - g(x)$ to find the next IMF.

The signal $s(x)$ is thus decomposed into intrinsic mode functions,

$$s(x) = \sum_{i=1}^{N} m_i(x) + R(x), \quad (1)$$

where N is the number of modes, $m_i(x)$ is the ith IMF from the decomposition, and R is the residue.

Each IMF has a well-behaved Hilbert transform. The signals can thus be transformed into a full energy-scale-frequency distribution $H(\omega, x)$, where ω assigns the frequency in the horizontal direction, and x is the distance. The Hilbert spectrum of the signal $h(\omega)$ is then given by

$$h(\omega) = \int_0^L H(\omega, w)\, \mathrm{d}x, \quad (2)$$

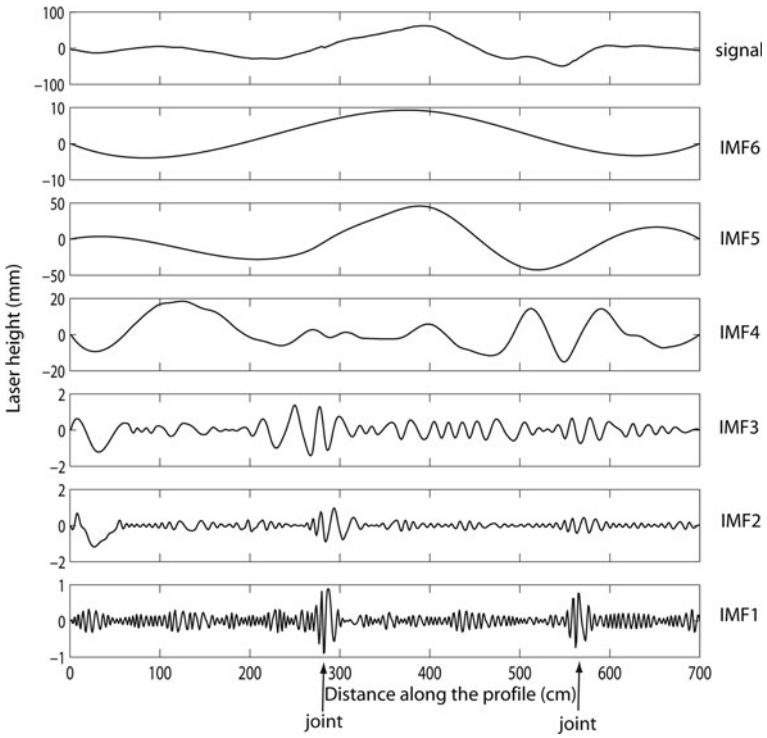

Fig. 4. EMD decomposition of the wooden plate profile shown in the top panel. The modes are represented from the bottom to the top. Modes 1–3 are notably different from modes 4–6.

where L is the length of the record. The highest frequency available is limited by the sampling rate, and is here 25 m^{-1}, corresponding to the smallest horizontal wavelength of 4 cm.

Signal on the wooden plate

EMD is applied to the five signals on the wooden plate. The decomposition yields between $N = 6$ and $N = 8$ IMFs (Fig. 4) and one residue (not shown). The EMD processing on the wooden plate shows that the number of IMF does not depend on the speed of the snowmobile, but only on the signal itself.

The 7 m wooden plate was composed of five plates of 1.40 m connected by hand, so that small discontinuities can exist at the interface between each plate. The analysis of the signal decomposition shows that the first modes have very different amplitude and frequency behaviour compared to the others (Fig. 4). We note that:

1. The amplitude of the signal formed by the sum of these first modes is within 1 mm, which is on the order of the engine vibrations, and

2. Discontinuities (1–3 mm high) at distances of 280 and 560 cm can be observed on these first modes, corresponding to the joints between each plate.

These two observations indicate that the first modes contain both the engine vibrations and the high-frequency part of the roughness signal. The decomposition shows that the last modes are composed of oscillations of greater amplitudes, thus representing the movement of the sledge on the snow.

The question is how to choose the exact number of modes to sum to separate the roughness signal and the snow-scooter movement. Note that the amplitudes and frequency spectrum between the first modes (corresponding to the roughness signal and the snow-scooter vibrations) and the last modes (corresponding to the snowmobile motion) change significantly, so that the correlation between these two classes of modes must change compared with the correlation across modes of the same class.

We note $s_M(x)$, the sum of the M first modes:

$$s_M(x) = \sum_{i=1}^{M} m_i(x). \tag{3}$$

We compute the correlation coefficient $r_p(M)$ between $s_M(x)$ and $s_{M+1}(x)$, for M varying between 1 and $N-1$:

$$r_p(M) = \frac{\sigma_{s_{M/M+1}}}{\sigma_{s_M} . \sigma_{s_{M+1}}}, \tag{4}$$

where σ_{s_M} and $\sigma_{s_{M+1}}$ are the variance of the functions $s_M(x)$ and $s_{M+1}(x)$, and $\sigma_{s_{M/M+1}}$ the covariance between $s_M(x)$ and $s_{M+1}(x)$. Mathematically, $r_p(M)$ expresses the correlation between two signals.

EMD divides the total signal into a sum of modes, where the lower modes have higher frequencies and lower amplitudes. The roughness signal will thus be contained in the first modes of the EMD, and the scooter motion will be contained in the last. Since the roughness signal and the motion of the snow scooter have different amplitude and frequency characteristics (Fig. 4), the correlation between one mode representing the roughness signal and the following one representing the scooter motion is low. By contrast, the correlation between two modes representing the same signal is high. This is why $r_p(M)$ increases as long as the modes M and $M+1$ are representative of the surface roughness, and drops suddenly when the two modes are not representative of the same signal. We use this criterion to subtract out the snowmobile movement.

We tested this method of correlation on the five-plate acquisition, and the resulting profiles are represented in

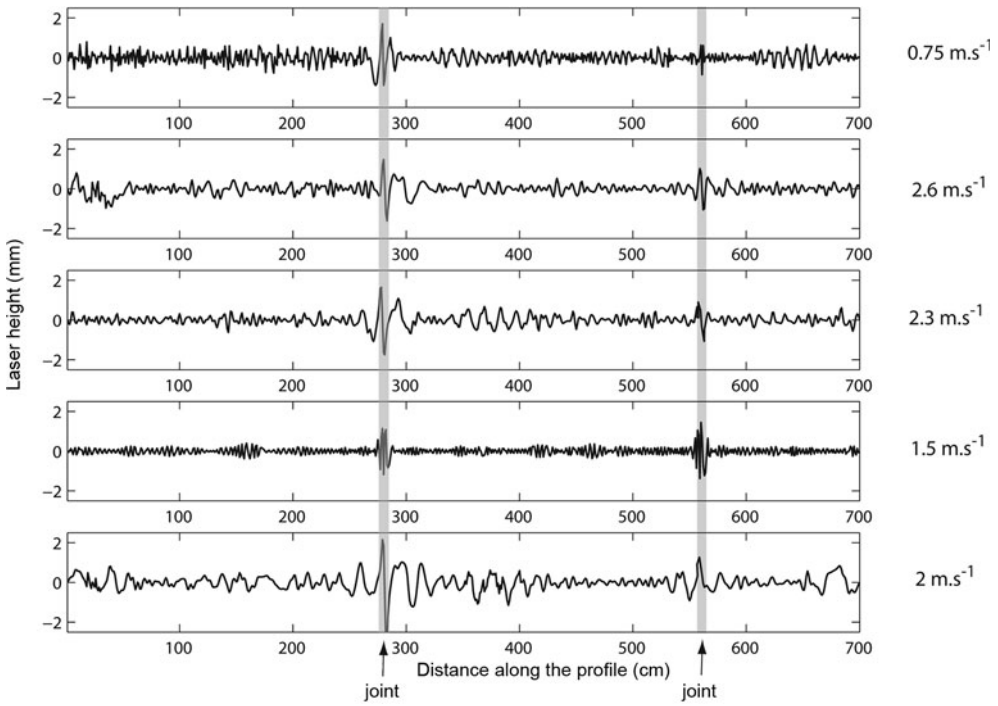

Fig. 5. Resulting signals for the five acquisitions on the board after subtracting the sledge movement. Snow-scooter velocity during the acquisitions is noted on the side of the profile.

Figure 5. The number of modes to sum, obtained with the correlation method, is 2.8 ± 0.4, not depending on the speed of the acquisition. The five profiles show exactly the same behavior, with a flat aspect on the plates (signal within 1 mm), and two discontinuities at the joints between the plates of 2–3 mm amplitude (Fig. 5). However, the resulting profiles have a lower noise for the two acquisitions obtained at lower speeds, 0.75 and 1.5 m s^{-1}. For the profiles acquired on the snow, the snow scooter has been driven at around 1 m s^{-1}, thus minimizing the noise.

Signal on the snow

The developed method, tested on the wooden board, is now applied to the snow surfaces. To compare the signals on the

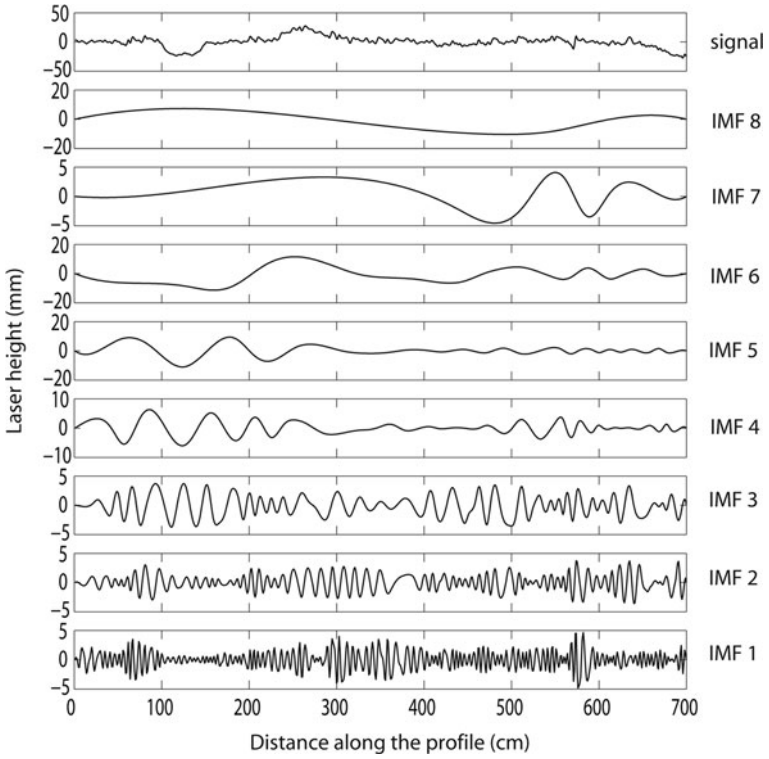

Fig. 6. Same as Figure 4, but for the snow profile.

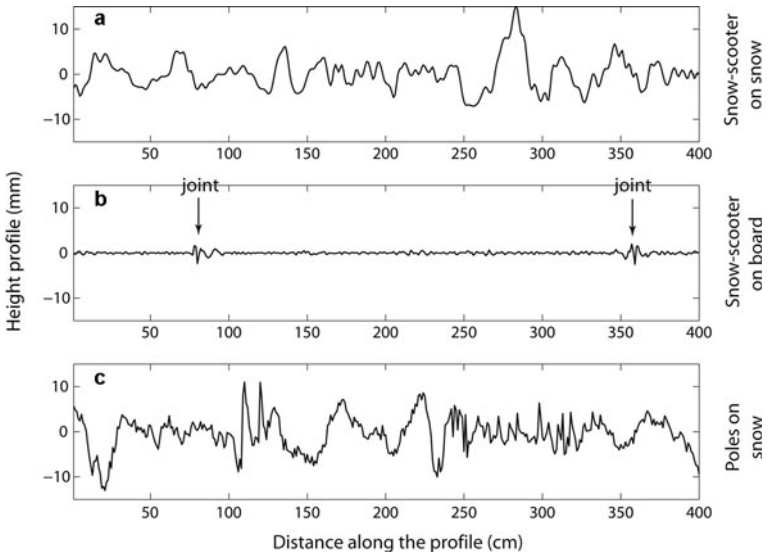

Fig. 7. (a, b) Profiles processed using the method described, on the snow (a) and on the wooden plate (b). (c) Profile on the snow obtained with the poles.

wooden plate and on the snow surface, we limit the length span to 7 m for the two surfaces. Thus the long downhill profile of 3200 m on the snow surface is split into many 7 m profiles. We apply the EMD to these profiles (Fig. 6). The decomposition yields $N = 7$ or $N = 8$ IMF components and one residue (not shown) from the data on the snow (Fig. 5).

We apply the correlation method to obtain the number of modes to sum; it is found to be 2–4 with a mean of 2.68 ± 0.7. The profile, with the snowmobile motion removed, is shown for the wooden plate and the snow surface in Figure 7. The standard deviation of the amplitude variations of the roughness signal is 0.5 mm on the wooden plate, and varies from 0.5 to 9.2 mm along the 3200 m snow profile. This standard deviation of 0.5 mm is consistent with the amplitude of the signal for a stationary but running snow scooter.

Since no direct comparison can be made between the obtained profiles, we first compare the profiles spectrum on the snow and on the board after separation of the roughness signal from the snowmobile motion (Fig. 8). The signals differ on the wooden plate and on the snow surface by more than 4 dB for all frequencies in the range 2–25 m^{-1}, but are the same for the snowmobile motion. The snowmobile is thus well extracted by the processing and we see that the snow surface-roughness signature has much greater amplitude than the vibrations. The EMD with these selected IMF components is used as a high-pass filter.

The uphill profile is computed in the same way as the downhill profile. The decomposition yields $N = 7$ or $N = 8$ IMF components and one residue from the snow data on the downhill profile. The roughness signal is obtained by adding either the 3 or 4 first modes with a mean of 3.4 ± 0.5. These higher values can be explained by the fact that we drove with much more power for the same speed on the uphill profile, thereby generating more high-frequency vibrations. As a result, the EMD decomposition contains an additional high-frequency mode compared to the downhill profile. The standard deviation of the amplitude variations varies from 0.5 to 8.6 mm along the 700 m. This range of variation is consistent with the values found on the downhill profile.

COMPARISON WITH LASER PROFILES ON POLES

Firstly, the three transects are filtered at 2 m^{-1} with a high-pass linear filter with cut-off frequency at 2 m^{-1}, to be compared with the snow-scooter profile. In this case the two spectra are similar (Fig. 3), and the signal amplitudes are comparable (Fig. 7). However, it is noticeable that the pole profiles contain more high-frequency signals. Indeed, the velocity of the laser was much lower on the poles than on the snow scooter, and consequently the sampling rate is higher, containing more high-frequency information than the profile achieved with the snow scooter. This high-frequency signal has very low amplitudes (<0.5 mm). The signal is characteristic of a lower scale of roughness (we will see later the fractal aspect of snow surfaces). Unfortunately, this scale of roughness cannot be retrieved by the snowmobile configuration. An increase of the sample rate would not necessarily enable us to reach this scale of roughness since higher-frequency signals also have lower amplitudes, which can be drowned by the snowmobile vibrations.

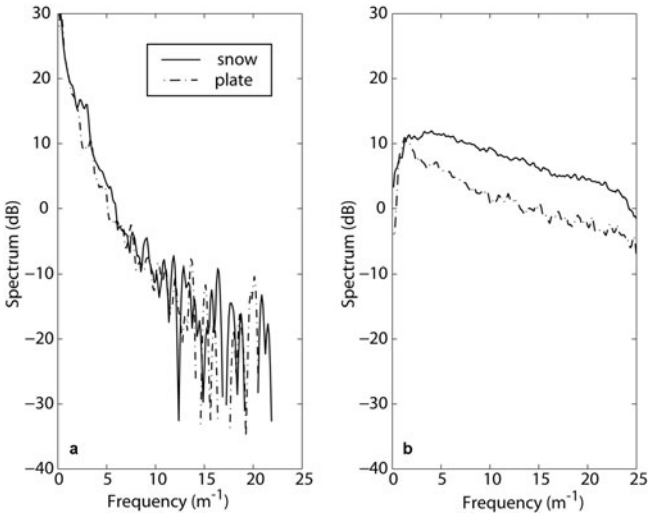

Fig. 8. Hilbert spectrum of modes 4–8 (a) and modes 1–3 (b).

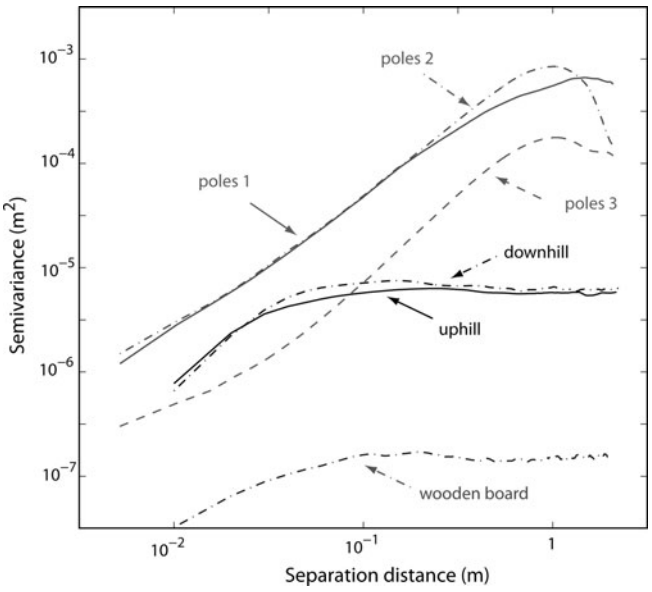

Fig. 9. Surface-roughness semivariograms for different profiles acquired with the laser: the laser translated onto the polels (top three traces), the laser pulled by the snow scooter over the snow (middle two traces), and the laser pulled by the snow scooter over the wooden board (bottom trace).

The pole transects have not been run exactly on the snowmobile profile track, and the profiles cannot be directly compared. In addition, the pole transects provide only three measurements of the snow surface distribution, which is certainly not enough to characterize the roughness statistics of the whole glacier. As a comparison, the number of 2 m profiles needed to characterize ploughed agricultural soils (well-organized surfaces) is four in each direction. We also notice that the laser measurements on board the scooter show a height-distribution RMS deviation (Table 1) of 0.5–9.2 mm, whereas the laser measurements on poles show a RMS height deviation of 2.7–6.7 mm.

The correlation length of the snow surface found with the pole measurements varies between 5 and 12 cm. In comparison, the correlation length found with the laser on board the snow scooter is 0.6–46 cm (Table 1), with most of the values being between 1 and 12 cm. This comparison shows the good agreement between the measurements done on the snow scooter and the profiles realized on the poles, and filtered to keep the same high-frequency signal.

DISCUSSION

Scale dependency of the surface roughness

The surface roughness is classically described by several parameters. The RMS height deviation σ_h is the RMS of the deviation of the surface height from its mean value. The autocorrelation length ℓ is associated with the autocorrelation function (ACF).

The calculation of these parameters has been shown to be dependent on the length of the profile (Arnold and Rees, 2003; Rees and Arnold, 2006), since the surface roughness is dependent on the scale of observation. We check this fractal-like surface aspect by calculating the roughness semivariogram (Fig. 9), which measures the semivariance of the surface height $\gamma(d)$ as a function of the spatial separation d between measurements i and j. The semivariogram is classically defined as

$$\gamma(d) = \frac{1}{2N(d)} \sum_{N(d)} (x_i - x_j)^2, \quad (5)$$

where $N(d)$ is the number of points separated by the distance d. See Arnold and Rees (2003), where a description and an analysis of the semivariogram can be found. The fractal dimension D of the surface is then obtained through the slope β of the best-fit line of the linear section of a logarithmic plot of semivariance and separation, where $\beta = 4 - 2D$ (Burrough, 1986).

Table 1. Classical roughness parameters, RMS height σ_h and correlation length l, calculated from the processed laser profiles

Parameter	Description	Min	Max	Mean	Std
σ_h (mm)	uphill	0.5	8.6	1.7	1.2
σ_h (mm)	downhill	0.5	9.2	1.8	1.0
σ_h (mm)	board	0.4	0.7	0.5	0.1
σ_h (mm)	pole	2.7	6.7	5.2	2.1
l (cm)	uphill	0.9	35.0	3.7	1.0
l (cm)	downhill	0.6	46.0	3.6	1.2
l (cm)	board	0.6	2.0	1.3	0.6
l (cm)	pole	5.0	12.0	7.9	2.0

The semivariograms for the different acquisitions (downhill, uphill, poles, wooden board) are presented in Figure 9. From the semivariogram on the poles, we note that surfaces have a fractal-like aspect at least until scales of 1.5 m. We also note that the three semivariograms, separated by at most 10 m, show a high variability of the surface roughness, indicating the need to acquire a great number of profiles to characterize the snow surface roughness. The fractal dimension of the profiles on the poles is, however, near constant, with $D = 1.33 \pm 0.05$. This low fractal dimension is characteristic of smooth surfaces.

The mean semivariograms for the uphill and downhill profiles are both very similar, with two main characteristics:

1. They present the same order of roughness as the profiles on poles for short scales of observation.
2. They show a threshold around 10 cm, above which the roughness no longer depends on the scales of observations. This threshold is explained by the high-pass filtering done with our signal processing. Indeed, we saw that scales of surface roughness of wavelength above 50 cm were eliminated, which has a strong impact on roughness parameter calculation of observations at large scales.

The fractal dimensions calculated from the downhill and uphill profiles are all situated between $D = 1.20$ and 1.50, with a mean of 1.37, which is close to the fractal dimension estimated from the poles profiles. The good agreement between the semivariograms at small scales obtained with the snow scooter and the poles for small scales of roughness validates both the measurement on the snow scooter and the developed signal processing for small scales of roughness. As a comparison, the semivariogram obtained from the profile on the board has much lower values of semivariance (Fig. 9).

Table 2. Comparison between classical roughness parameters, RMS height σ_h and correlation length l, for different measurements done on snow surfaces

Parameter	Rott (1984)	Williams and others (1988)	Arnold and Rees (2003)	Rees and Arnold (2003)	This work
Season	Summer	Winter	Spring	Summer	Spring
Location	Austrian Alps	Bavarian Alps	Svalbard	Svalbard	Svalbard
σ_h (mm)	6.1 ± 2.4	0.3 – 1.5	2.1	6.9	1.8 ± 1
l (cm)	9.1 ± 5.6	–	–	–	3.7 ± 1

Roughness parameters

For radar analysis purpose and aerodynamic roughness studies, and because of the fractal aspect of snow surfaces, Rees and Arnold (2006) advise calculation of the snow surface-roughness parameters over short transects of a few metres sampled every centimetre. Figure 8 shows that measurements with the laser on board the snow scooter are equivalent to several 10 cm long transects. However, we saw previously that the laser measurements allow a restitution of topographic scales until 50 cm wavelengths, which is very well adapted for radar return analysis (wavelength of 5.6 cm at C band).

We check that the surface height distribution is Gaussian, which is visually the case. We calculate σ_h and ℓ, on profile sections of 1.5 m, over the whole downhill and uphill profiles. The two profiles are never separated by >30 m, but their roughness statistics are highly variable at the metre scale, so the measurements cannot actually be compared along the profile. However, their range of variation matches well (Table 1).

The σ_h values are found between 0.5 and 9.2 mm, with a mean of 1.8 ± 1 mm for this glacier (Table 1). Such low values were expected because of the smooth aspect of the snow surfaces. We notice significant variability of the roughness parameters at the metre scale. This observation is also in good agreement with the observations made in the field. For instance, the three pole transects are within 10 m of each other, but their σ_h vary between 2.7 and 6.7 mm. The sensors on board satellites usually have a much lower resolution and this variability should be taken into account when characterizing the mean roughness parameters over satellite footprints.

The correlation length ℓ of the snow surface is found to be between 0.6 and 46 cm, with a mean of 3.6 ± 1.2 cm (Table 1). As a comparison, Rees and Arnold (2006) report the correlation length of a snow-free glacier, which shows the major contribution to the C-band radar, to be $\sim$6 cm.

Table 2 summarizes some of the previous measurements (Rott, 1984; Williams and others, 1988; Arnold and Rees, 2003) of surface roughness carried out on snow. The comparison is not obvious, since snow conditions for the different studies varied. Moreover, seasonal differences can occur, with smoother surfaces in the spring (Arnold and Rees, 2003). However, comparison with these previous works shows that the range of measurements performed with the laser on board the snow scooter compares well with measurements by other techniques. For instance, the measurements by Arnold and Rees (2003) on the same glacier in the same season (spring), using a black plate, show RMS height deviation of 2.1 ± 0.0043 mm, very close to the 1.8 ± 1 mm found in this study.

CONCLUSION

We demonstrate the possibility of easily retrieving snow profiles over long distances by operating a laser device fixed onto a snow scooter. We first operate the device on a flat surface to estimate the snow-scooter vibrations, both in frequency and in amplitude. For the snow scooter used here, the scales of roughness that can be retrieved are in the range 4–50 cm for horizontal wavelength with a vertical amplitude of >1 mm.

The snow scooter moves with the metre-scale topography, making it necessary to decouple this low-frequency signal and the small-scale roughness signature. The snow-scooter signal can be subtracted by a scale-frequency analysis. We use an EMD decomposition that is very well adapted to non-stationary data and allows us to compute the Hilbert transform. The EMD is used here as a means of non-linear high-pass filtering. The number of IMF components, to choose from the decomposition to reconstruct the roughness signal, can be found by a correlation method. This processing is validated by comparison with profiles acquired with the laser on two parallel poles. This comparison shows that the laser profiler on the snow scooter is equivalent to multiple transects around 10 cm long, characterizing scales of roughness up to 50 cm of wavelength.

The laser provides the roughness spectrum up to 50 cm, whereas the GPS operated at the same time on board the snowmobile at 1 Hz (with a speed of 1 m s^{-1}) can provide the roughness spectrum from a 2 m wavelength. The whole spectrum cannot be retrieved completely by this method. In the future, the range of validity of the method might be improved through different possibilities:

1. the use of a GPS coupled with a inertial navigation system, in order to estimate the motion of the sledge and correct the laser measurements from the long wavelength effects;
2. an increase in the sampling rate of the GPS measurements to fill the gap between the laser and GPS range. GPS measurements at 10 Hz can already be undertaken.

However, for the first time the roughness of snow surfaces at millimetre and centimetre scales can be measured over large profiles, providing the variation range of the snow surface-roughness parameters, σ_h and ℓ. The roughness parameters are found to vary very quickly over short distances. For these relatively smooth surfaces (no satrugi), the classical roughness parameters are found to be in the 0.5–9.2 mm range for the RMS height distribution, and in the 0.6–46 cm range for the correlation length. The measurements undertaken on midre Lovénbreen are representative of smooth surfaces.

Rees and Arnold (2006) report that the correlation length of a snow-free glacier that makes a major contribution to the C-band radar is 6–7 cm. Hence, a laser on board a snow scooter is particularly well adapted for studying micro-roughness of snow surfaces, in the range of interest for GHz radars. This device can be used in the future for a wide variety of microwave remote-sensing applications on snow, for improved analysis of SAR or altimetric data. Of particular interest here are the calibrations of altimetric data (Envisat, CryoSat) over ice sheets that are sensitive to this parameter. This instrument is also of particular interest for surface energy-balance studies, since aerodynamic roughness length can also be derived from measurements of snow profiles at millimetre and centimetre scales (Bagnold, 1941; Lettau, 1969; Munro, 1989).

The laser has recently successfully been used at Dome C, Antarctica, in February 2008, under much rougher conditions than on midre Lovénbreen. We hope that the relative simplicity of this instrument will convince research scientists to use it at different locations, to improve knowledge of snow-surface roughness.

ACKNOWLEDGEMENTS

This work is a contribution to the ENVITOOLS and the PIRLETA (Profiler Instrument for Roughness estimate using a Laser Easy To Adapt) project. The paper benefited from the comments of two anonymous reviewers.

REFERENCES

Albert, M.R. and R.L. Hawley. 2002. Seasonal changes in snow surface roughness characteristics at Summit, Greenland: implications for snow and firn ventilation. *Ann. Glaciol.,* **35**, 510–514.

Arnold, N.S. and W.G. Rees. 2003. Self-similarity in glacier surface characteristics. *J. Glaciol.,* **49**(167), 547–554.

Bagnold, R.A. 1941. *The physics of blown sand and desert dunes.* London, Methuen and Co.

Bindschadler, R., H. Choi, C. Shuman and T. Markus. 2005. Detecting and measuring new snow accumulation on ice sheets by satellite remote sensing. *Remote Sens. Environ.,* **98**(4), 388–402.

Bingham, A.W. 1997. Monitoring Arctic glaciers and ice caps using satellite remote sensing. (PhD thesis, University of Cambridge.)

Burrough, P.A. 1986. *Principles of geographical information systems for land resources assessment.* Oxford, Clarendon Press.

Davidson, M.W.J., T. Le Toan, F. Mattia, C. Satalino, T. Manninen and M. Borgeaud. 2000. On the characterization of agricultural soil roughness for radar remote sensing studies. *IEEE Trans. Geosci. Remote Sens.,* **38**(2), 630–640.

Furukawa, T. and N.W. Young. 1997. Comparison of microwave backscatter measurements with observed roughness of the snow surface in East Queen Maud Land, Antarctica. *In* Guyenne, T.D. and D. Danesy, *comp. Proceedings of the 3rd ERS Symposium on Space at the Service of Our Environment, 17–21 March 1997, Florence, Italy, Vol. 1.* Noordwijk, European Space Agency, 803–807.

Gloersen, P. and N. Huang. 2003. Comparison of interannual intrinsic modes in hemispheric sea ice covers and other geophysical parameters. *IEEE Trans. Geosci. Remote Sens.,* **41**(5), 1062–1074.

Grandjean, G., P. Paillou, P. Dubois-Fernandez, T. August-Bernex, N.N. Baghdadi and J. Achache. 2001. Subsurface structures detection by combining L-band polarimetric SAR and GPR data: example of the Pyla Dune (France). *IEEE Trans. Geosci. Remote Sens.,* **39**(6), 1245–1258.

Herzfeld, U.C., H. Mayer, N. Caine, M. Losleben and T. Erbrecht. 2003. Morphogenesis of typical winter and summer snow surface patterns in a continental alpine environment. *Hydrol. Process.,* **17**(3), 619–649.

Huang, N.E. *and 8 others.* 1998. The empirical mode decomposition and the Hilbert spectrum for nonlinear and non-stationary time series analysis. *Proc. R. Soc. London, Ser. A,* **454**(1971), 903–995.

Hwang, P.A., N.E. Huang and D.W. Wang. 2003. A note on analyzing nonlinear and nonstationary ocean wave data. *Appl. Ocean Res.,* **25**(4), 187–193**.**

Lacroix, P., B. Legrésy, R. Coleman, M. Dechambre and F. Rémy. 2007. Dual-frequency altimeter signal from Envisat on the Amery ice-shelf. *Remote Sens. Environ.,* **109**(3), 285–294.

Lacroix, P., M. Dechambre, B. Legrésy, F. Blarel and F. Rémy. 2008. On the use of the dual-frequency ENVISAT altimeter to determine snowpack properties of the Antarctic ice sheet. *Remote Sens. Environ.,* **112**(4), 1712–1729.

Legrésy, B. and F. Rémy. 1997. Altimetric observations of surface characteristics of the Antarctic ice sheet. *J. Glaciol.,* **43**(144), 265–275.

Lettau, H. 1969. Note on aerodynamic roughness-parameter estimation on the basis of roughness element description. *J. Appl. Meteorol.,* **8**(5), 828–832.

Molla, M.K.I., M.S. Rayman, A. Sumi and P. Banik. 2006. Empirical mode decomposition analysis of climate changes with special reference to rainfall data. *Discrete Dyn. Nature Soc.,* **2006**, 45348.

Munro, D.S. 1989. Surface roughness and bulk heat transfer on a glacier: comparison with eddy correlation. *J. Glaciol.,* **35**(121), 343–348.

Oveisgharan, S. and H.A. Zebker. 2007. Estimating snow accumulation from InSAR correlation observations. *IEEE Trans. Geosci. Remote Sens.,* **45**(1), 10–20.

Rees, W.G. 1998. Correspondence. A rapid method for measuring snow surface profiles. *J. Glaciol.,* **44**(148), 674–675.

Rees, W.G. and N.S. Arnold. 2006. Scale-dependent roughness of a glacier surface: implications for radar backscatter and aerodynamic roughness modelling. *J. Glaciol.,* **52**(177), 214–222.

Ridley, J. and K. Partington. 1988. A model of satellite radar altimeter return from ice sheets. *Int. J. Remote Sensing,* **9**(4), 601–624.

Rott, H. 1984. The analysis of backscattering properties of SAR data of mountain regions. *IEEE J. Ocean. Eng.,* **9**(5), 347–355.

Ulaby, F.T., R.K. Moore and A.K. Fung. 1982. *Microwave remote sensing, active and passive. Vol. 2: Radar remote sensing and surface scattering and emission theory.* Reading, MA, Addison-Wesley.

Williams, L.D., J.G. Gallagher, D.E. Sugden and R.V. Birnie. 1988. Surface snow properties effects on millimeter-wave backscatter. *IEEE Trans. Geosci. Remote Sens.,* **26**(3), 300–306.

Zhang, R.R., S. Ma and S. Hartzell. 2003. Signatures of the seismic source in EMD-based characterization of the 1994 Northridge, California, earthquake recordings. *Bull. Seismol. Soc. Am.,* **93**(1), 501–518.

MS received 27 November 2007 and accepted in revised form 6 June 2008